ISSN 1027-4510, Journal of Surface Investigation: X-ray, Synchrotron and Neutron Techniques, 2024, Vol. 18, Suppl. 1, pp. S302–S310. © Pleiades Publishing, Ltd., 2024.

Defect Formation and Displacement of Atoms on the Surface of a LiF Crystal under Bombardment with Low-Energy Cesium Ions

U. B. Sharopov[a, b, *], O. A. Abdulkhaev[a], B. E. Egamberdiev[a], K. A. Samiev[b], N. M. Nazarova[b], M. K. Kurbanov[c], M. K. Karimov[c], D. S. Saidov[d], Z. I. Iskandarov[e], S. Y. Islamov[e], A. R. Kakhramonov[f], O. E. Abdurakhmonov[j], I. A. Pronin[h], and A. S. Komolov[i]

[a] *Physical-Technical Institute, Uzbekistan Academy of Sciences, Tashkent, 100084 Uzbekistan*

[b] *Bukhara State University, Bukhara, 20008 Uzbekistan*

[c] *Urgench State University, Urgench, 220100 Uzbekistan*

[d] *Urgench branch of the Tashkent University of Information Technologies, Urgench, 220100 Uzbekistan*

[e] *Tashkent State Agrarian University, Tashkent, 111218 Uzbekistan*

[f] *Institute of Materials Science, Tashkent, 102226 Uzbekistan*

[j] *Tashkent Institute of Chemical Technology, Tashkent, 100011 Uzbekistan*

[h] *Penza State University, Penza, 440026 Russia*

[i] *St. Petersburg State University, St. Petersburg, 1999034 Russia*

**e-mail: utkirstar@gmail.com*

Received May 15, 2024; revised July 15, 2024; accepted July 25, 2024

Abstract—Ion beam technology is an excellent tool for changing and investigating the structural and surface properties of crystals. In this paper, the possibility of modifying the surface of a thin LiF film under irradiation with low-energy Cs ions with an energy of 1 keV using the SRIM software method is investigated. The results of the study show that the average range of cesium ions is 51 Å, and the average surface binding energy is 2.8 eV. Due to the transfer and distribution of the energy of bombarding ions to the atomic lattice and as a result of the displacement of the lattice atoms from their initial positions, it is possible to obtain the value of displacement defects. The defect formation profile was investigated depending on DPA, which implies that the maximum peaks of defect displacement for LiF are at a crystal depth of 16 Å from the surface.

Keywords: lithium fluoride, low-energy ions, SRIM, thin films, ion irradiation, surface

DOI: 10.1134/S1027451024702215

INTRODUCTION

Optical crystals have gained great popularity as a material for various radiation technological purposes due to their interesting lattice structural properties, which depend on the local arrangement of atoms [1–6]. At the same time, these structural features can be modified by changing the local arrangement of atoms in the crystal lattice using various methods based on the specifics of the application and application [7–10]. One of these methods is the diffusion of atoms on the surface [11–13]. The method of diffusion from the surface to the volume of a solid has its disadvantages, the main of which is the low diffusion rate, especially at low temperatures [14, 15]. Another equally effective method is ion beam technology [16, 17], which uses ions of different energies to process materials [18, 19]. Also, ion beam etching remains an indispensable tool for surface cleaning [20]. Various ion sources are used, including gas discharges, particle accelerators and nuclear reactors [21]. During such processing, enormous energy is transferred to the material through the electron-phonon interaction [22, 23]. The advantage over other material processing methods is that it allows materials to be processed with high precision and reproducibility. This makes ion beam technology ideal for applications where high precision is required, for example, for the manufacture of microchips or optical components, as well as for processing materials that are brittle or sensitive to heat [16, 24, 25]. One such material is lithium fluoride, with a wide range of applications in radiation technology [26]. The crystal has a number of properties—high dielectric strength and good transparency, which make it ideal for radiation applications. LiF crystals are used as protection against the effects of X-ray radiation [3, 27], and are also used as neutron [28], X-ray and gamma radiation detectors to obtain images of organs and tissues [29].

Any irradiation of a solid results in a huge energy release, which displaces the atoms of the lattice from their original positions, and such displacement of

atoms ultimately causes stress in the geometry of the crystal lattice, a phenomenon called structural modification [30, 31]. Structural modification causes the formation of vacancies and point defects in the regular crystal lattice [32, 33]. But the use of low-energy ions when modifying the surface of crystals is often not attractive due to the small penetration depth and long irradiation time [34–37]. Analysis of collision events provides detailed information about the displacement of atoms. When atoms collide, energy and momentum are exchanged. As a result, atoms can be displaced from their positions in the crystal lattice. Analysis of collision events also allows one to determine the parameters of atomic displacement, vacancies and defects [38]. Moreover, the analysis of collision events also provides results on the formation of defects along the displacement directions, which carry important information in the context of ion bombardment. In addition, the collision cascade increases the surface sputtering efficiency, which can be used for surface modification. Thus, bombarding a surface with atomic particles can be used as a powerful tool to engineer a defective sample surface followed by modification (etching, diffusion, defect engineering). Previous work has shown that the SRIM software product indeed complements, visualizes and explains some inexplicable physical phenomena obtained experimentally [32]. In this work, the effect of low-energy (1 keV) Cs ions on a thin film of LiF crystals was studied. The purpose of this study is to study the interaction and influence of heavy low-energy ions on the modification of the surface region of the sample using a technique for modeling the interaction of ions with matter. The data obtained in this work can serve to test the mechanisms of defect formation and modification of the surface region of ionic crystals using low-energy ions and to compare previous experimental works [32, 39].

MODELING TECHNIQUE

The SRIM/TRIM (Stopping and Range of Ions in Matter/Transport of Ions in Matter) program is a software for modeling the interaction of ions with matter [40]. She uses the Monte Carlo method to track the trajectory of an ion in a substance. We used the SRIM/TRIM software package to study surface and structural modifications of LiF based on the sputtering coefficient and the surface binding energy of atoms. Experimental data on the parameters of the LiF crystal were used as initial data for modeling.

The following parameters were used to simulate the process:

Crystal type and structure: LiF-cubic face-centered, lattice parameter: 4.020 Å, lithium atom mass – 6.941 amu, fluorine atom mass—18.998 amu, cesium ion mass—132.905 amu, target density—2.635 g/cm^3 = 1.2235×10^{23} at/cm^3.

During the simulation process, data about the bombarding ion, the substance, and collision conditions are entered into the SRIM program. The program calculates the ion's trajectory in the material using the Monte Carlo method and outputs simulation results, such as the ions energy, its position, and direction of movement. Figure 1 presents the visual environment of the SRIM program – the formation of defects and the range of cesium ions through the depth of the LiF crystal at a 0° angle relative to the surface normal with an energy of 1 keV. From the figure, one can obtain the range of cesium ions in the LiF sample, and based on a detailed collision event, an estimate can be given on the data about energy release. Also, in TRIM mode, the program shows how bombarding cesium ions displace lattice atoms from their original positions, thereby creating vacancies and point defects in the periodic arrangement of the LiF crystal. Furthermore, the displacement cross-section value of atoms and their impact on the modification and structural properties of the sample surface were determined and analyzed based on displacement defects, as a result of bombardment with heavy low-energy ions. The distribution profile of vacancies, interstitial defects, and substitution atoms from the surface to the depth of displacement in the sample was also studied.

Analyzing the sequence of collisions, information can be obtained about the creation of displaced atoms, interstitial defects, substitution atoms, and vacancies. Thus, during the collision events, there is a transfer of energy from the ions to the sample, leading to surface and bulk damage in LiF. Finally, the distribution of damage was studied from the perspective of the defects created in LiF crystals during the bombardment with Cs ions, providing information on the depth of interstitial defects in the sample, to which such damage reaches and creates substitution defects and vacancies.

In this study, to investigate the damages caused by the impact of Cs ions with an energy of 1keV on LiF crystals, a full-stage calculation was conducted based on the Kinchin-Pease model [41]. During the simulation, the thickness of the LiF film was set to 150 Å, cesium ion energy to 1 keV, and displacement energy and bond energy to 25 and 3 eV, respectively, which are very important parameters for the study of surface sputtering.

As is known, the SRIM/TRIM software is used to understand the interaction of different ions with various samples, which is based on Monte Carlo simulation using the binary collision approximation [42]. This method predicts the range of bombarding ions, the ion deceleration process, energy release, and other physical properties, such as information on atomic recoil damage and sputtering.

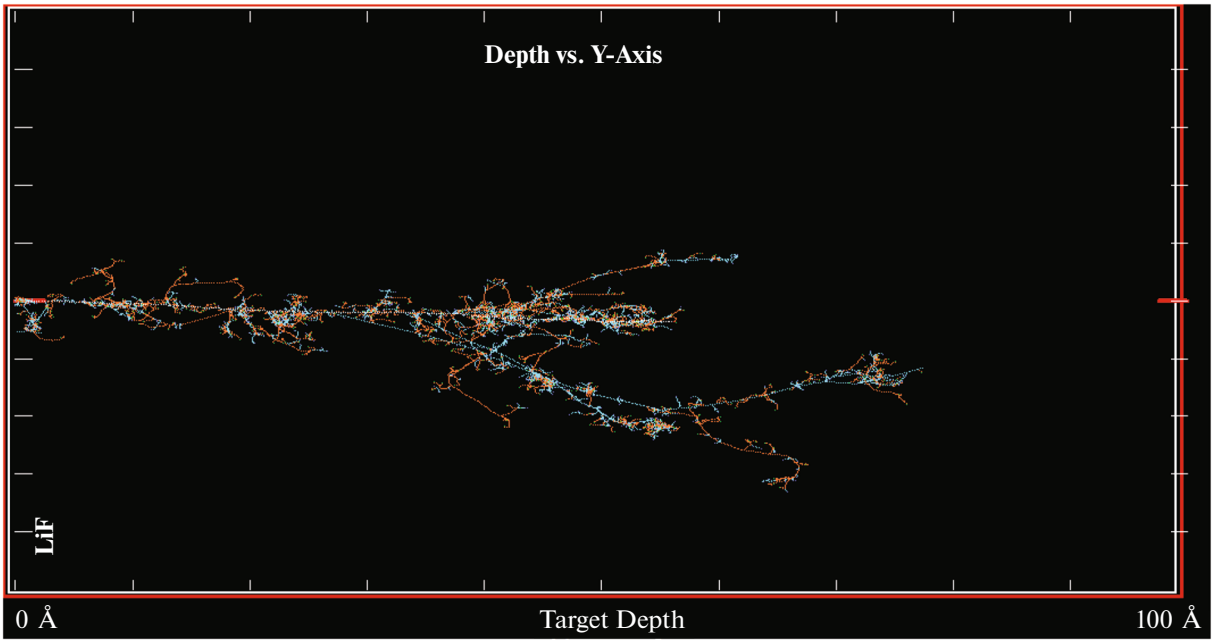

Fig. 1. Visual environment of the SRIM program for the formation of defects and the run of cesium ions along the depth of the LiF crystal at an angle of 0° relative to the surface normal with an energy of 1 keV, obtained by computer simulation of atomic collisions.

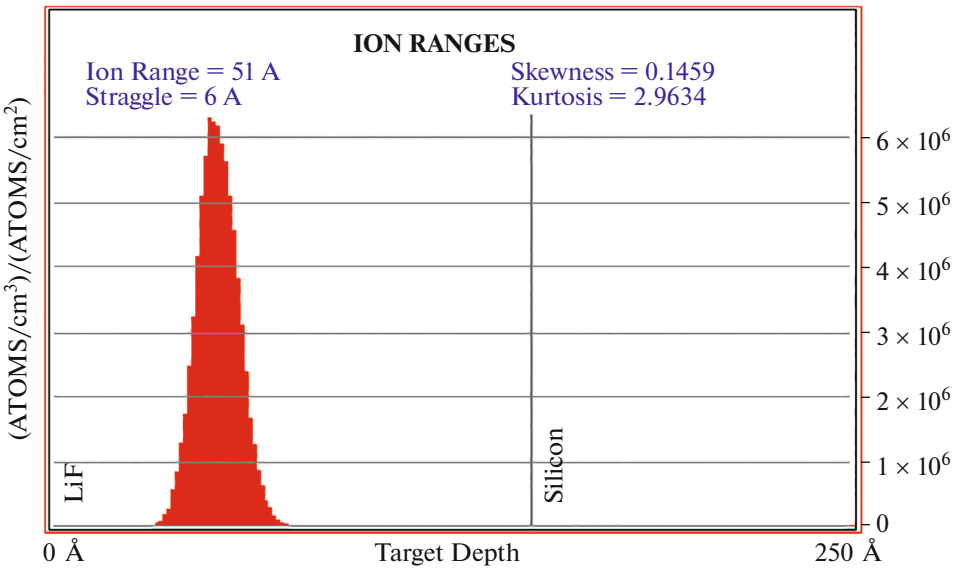

Fig. 2. The profile of the cesium ion path along the depth of the LiF crystal under irradiation with an energy of 1 keV.

RESULTS AND DISCUSSION

As shown in Fig. 1, the range of cesium ions at a 0° angle relative to the surface normal with an energy of 1 keV penetrates the volume of the LiF crystal up to a depth of approximately 34–75 Å (this can also be confirmed from Fig. 2). Simultaneously, displacement defects (green dots) of lithium ions, vacancies of lithium atoms (brown dots), displacement defects (light blue dots) of fluorine ions, vacancies of fluorine atoms (dark blue dots), and substitution defects of cesium ions (red dots) are formed.

Based on the physics of the elastic collision of two particles, each time cesium with an energy of 1 keV strikes a fluorine or lithium atom, it transfers a significant portion of its energy, resulting in a collision cascade (Fig. 1). After the ion changes direction, the parent atom rebounds due to the cascade (forming dis-

placement defects—green dots), and all its subsequent collisions result in the formation of vacancies, displayed as blue dots. Thus, one atom from the cascade creates more than 21 vacancies along its path.

It is known that during the bombardment of ions with the surface of crystals, phenomena such as ionization, electronic excitation, defect formation, sputtering, etc., occur. An important factor in stimulating sputtering is the formation of defects. The higher the concentration of defects, the higher the sputtering coefficient and the more effective the surface erosion. The quantitative character of the sputtering coefficient K_{Sp} of materials can be expressed in terms of the number of sputtered or secondary atoms (N_{Se}) by one ion (N_{Pr}):

$$K_{Sp} = N_{Se}/N_{Pr}, \quad (1)$$

where N_{Se} is the number of sputtered or secondary atoms; N_{Pr} is the number of incoming ions.

According to Sigmund's theory, the sputtering coefficient depends on the electronic and nuclear stopping powers, as well as on the mass of the incoming ion [43]. According to our SRIM results, the corresponding average range of cesium ions in lithium fluoride crystal is about 51 Å (Fig. 2). This means that the main concentration of cesium-induced defects is focused at a depth of 51 Å within the LiF crystal. Moreover, this sputtering is also associated with the energy released during deceleration on the electronic shells and nuclei of ions. The calculations obtained from SRIM show that for cesium ions at an energy of 1 keV, the deceleration on electronic shells equals—1.7 eV/Å.

$$dE/dx_{Elec} = 1.7 \text{ eV/Å}.$$

Also, for cesium ions at an energy of 1 keV, the deceleration on nuclei corresponds to:

$$dE/dx_{Nucl} = 61.8 \text{ eV/Å}.$$

As evident, the deceleration of cesium ions on the nuclei of the sample is 36 times greater than on the electron cloud.

Thus, in the case of irradiation with Cs ions at an energy of 1 keV, atoms of the LiF crystalline structure are displaced from their positions due to the redistribution of energy release, initiating a cascade of collisions with the displacement of lithium and fluorine atoms. During the collision cascade, some atoms are also repelled, contributing to the phenomenon of surface sputtering. Moreover, some atoms, due to recoil cascades, return from the bulk to the surface and, after transferring their energy to surface atoms, destroy the surface binding energy that holds fluorine and lithium atoms on the surface. Figure 3 shows the distribution profile of absorbed energy by lithium and fluorine lattice atoms in the LiF crystal depth from bombarding cesium ions with an energy of 1 keV. As we have already stated, the energy of bombarding cesium ions, approximately 810 eV, is distributed among the lattice atoms during the collision. On the surface, lithium atoms receive energy from cesium ions of 221 eV, and fluorine ions receive approximately 620 eV; the transferred energy decreases to zero at a crystal depth of 30–40 Å. This means that the cesium ion, upon contact with the surface, begins to transfer its energy and stops at a depth of the crystal of 34–75 Å (Fig. 2).

Surface binding energy is the energy that binds atoms together near the surface, necessary for removing lithium or fluorine atoms from the crystal surface. The value of the surface binding energy of LiF, obtained by ion sputtering methods, is about 2.8–3.2 eV [44]. When the energy received is higher than this value, surface sputtering occurs. Therefore, the sputtering process depends on this surface binding energy, which must be lower than the energy of the incoming ion or the energy of the ion cascade. We obtained the average surface binding energy directly from the TRIM results. If the energy of recoil atoms is sufficient to break the valence surface bonds, as shown in Fig. 4, which is 2.8 eV, then with increasing energy of the cascade atom, the valence surface bond breaks, and an atom or molecule detaches from the solid surface and leaves the sample surface. As seen, the distribution of excited atoms below 2.8 eV is very high, but this energy is insufficient for sputtering from the surface. This means that to detach a lithium or fluorine atom from the LiF surface, the recoil atom's energy must be at least 2.8 eV (Fig. 4). Finally, the recoil atom's energy for breaking valence surface bonds depends on the mass of the primary ion. Thus, by choosing a suitable heavy ion, one can easily determine the average surface binding energy. This makes irradiation ions a suitable tool for surface processing.

The interaction of cesium ions with the atoms of the LiF sample can be analyzed based on collision events, as these collisions lead to the formation of defects and displacement of atoms from their regular positions in the lattice. Considering each collision event is very important, as the primary Cs atom changes its trajectory when it encounters LiF atoms, due to elastic (nuclear) and inelastic (electronic) scattering, as mentioned above. The trajectory direction depends on the atomic density in the LiF crystal lattice, as well as on the electronic-nuclear stopping power of cesium.

After a collision event, the lattice atoms of fluorine and lithium are displaced from their original positions, which can cause the formation of various types of lattice defects, such as point defects, vacancies, displacement defects, and substitution defects. Defects formed during ion irradiation directly affect the structural properties of the crystal surface. Thus, the distribution of formed displacement defects, vacancies, and substitutions can be represented depending on the depth of formation in LiF, as shown in Fig. 5.

The displacement of target atoms can be defined as the total sum of fluorine and lithium vacancies of the target, or can be referred to as the target components,

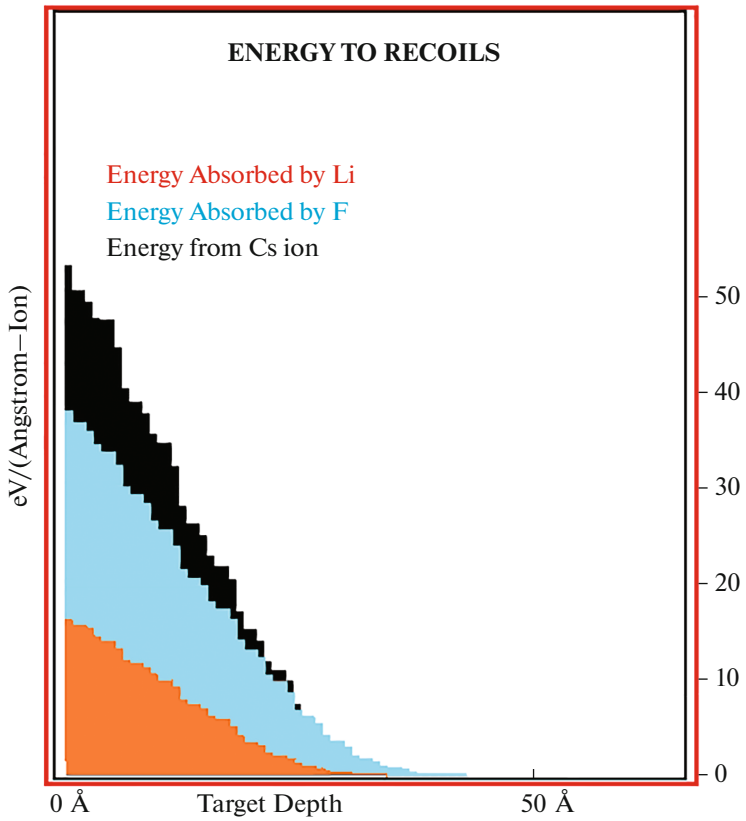

Fig. 3. Depth distribution profile of the adsorbed energy of bombarding cesium ions with an energy of 1 keV on lithium fluoride lattice atoms.

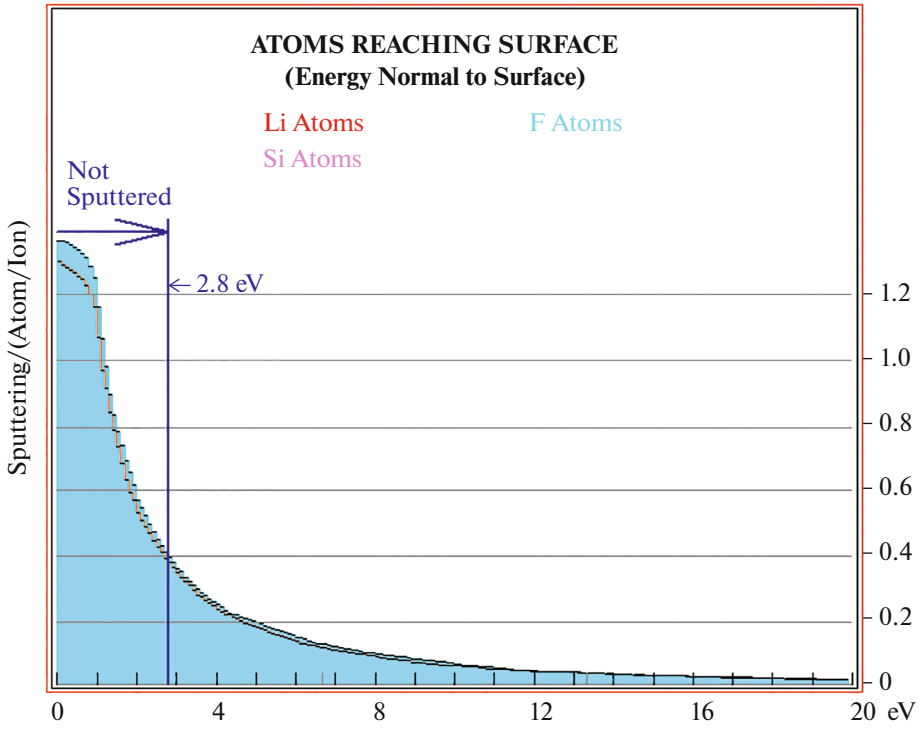

Fig. 4. Sputtering yield profile of irradiated LiF crystals with cesium ions.

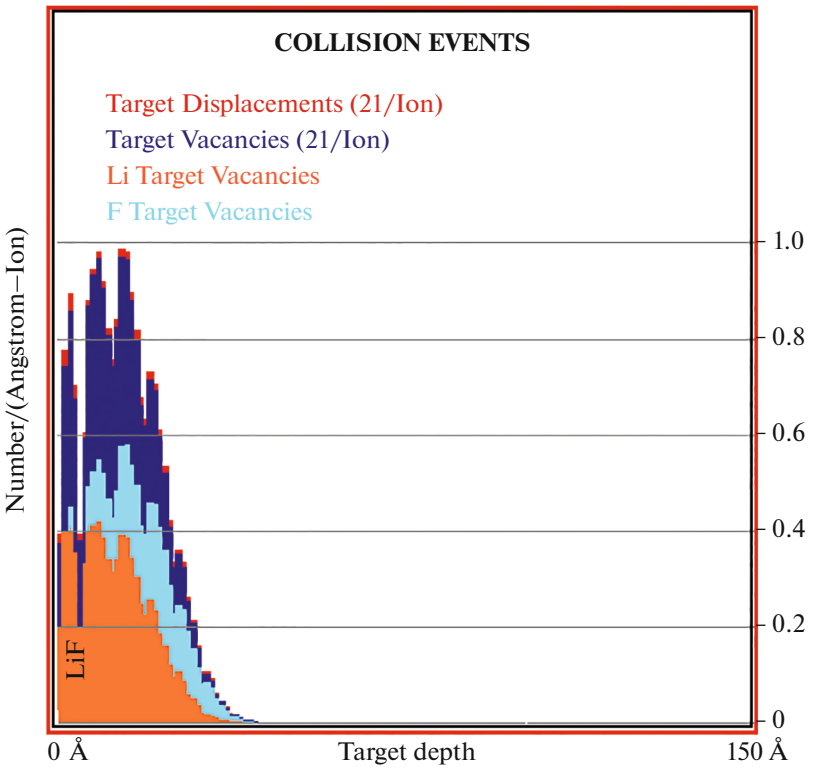

Fig. 5. Distribution of defects formed after collision with cesium ions with an energy of 1 keV of LiF crystals depending on the depth of the sample.

as well as substituting collision atoms. From the SRIM program, not only the concentration of target vacancies and substituting collision atoms can be obtained, but also information about displacement defects. Displacement defects are defects caused by the displacement of lithium and fluorine atoms. Figure 5 shows the total number of defects formed due to collision, obtained from SRIM. As seen, the highest concentration of defects is associated with the displacement of target atoms (red). The second place is taken by vacancies of target atoms (dark blue), and subsequent lower concentrations correspond to fluorine vacancies (light blue) and lithium vacancies (brown). The curves show that displacement defects of the parent crystal are formed first, after which vacancies are formed, hence their concentration is the same.

The distribution of defects on the surface can be represented as a function of displacement per incident atom (DPA). DPA is a unit of measurement for radiation damage to materials when modifying surfaces with ions. DPA is used to create defects on surfaces for research or manufacturing purposes to improve or damage surfaces. DPA indicates the average number of atoms displaced from the crystal lattice node due to bombardment.

DPA is a dimensionless quantity and is usually expressed as a fraction of 1. Ion doses can be converted to equivalent displacement dose D in units of displacement per atom (DPA) at the peak of damage, which is given by the following formula:

$$D = \left[\frac{N^*_{\text{dis}}}{N}\right]\Phi. \quad (2)$$

To determine DPA, we first need to calculate the cross section of displaced defects σ_{SRIM}, which can be determined by the following formula (3) and the dose of incident ions Φ.

Thus, the displacement cross section σ_{SRIM} can be obtained through the ratio of the number of displacement defects to the atomic density of the crystal (3),

$$\sigma_{\text{SRIM}} = \left[\frac{N^*_{\text{dis}}}{N}\right], \quad (3)$$

where N^*_{dis} is the number of displacement defects per ion and per 1 Å—unit length, which is determined by the sum of vacancies and displacement defects. N is the atomic density of LiF crystals, which is equal to—1.22×10^{23} at/cm^3 or 122 at/nm^3. Then the displacement cross section σ_{SRIM} will look like in Fig. 6.

The cross-sectional profile of the formed displaced defects directly depends on the dose of incident radiation and the penetration depth of ions. To determine the dose of incident cesium ions, the following

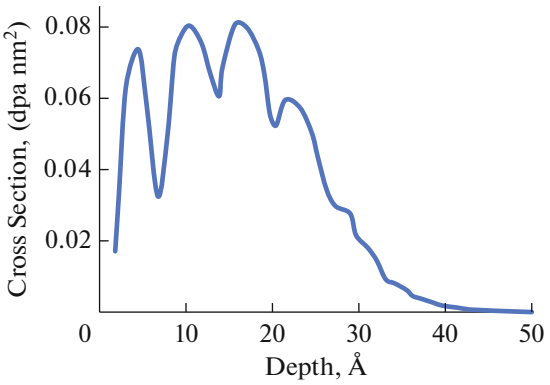

Fig. 6. Cross-sectional profile of the formed displaced defects depending on the depth of the LiF sample at irradiation with Cs ions.

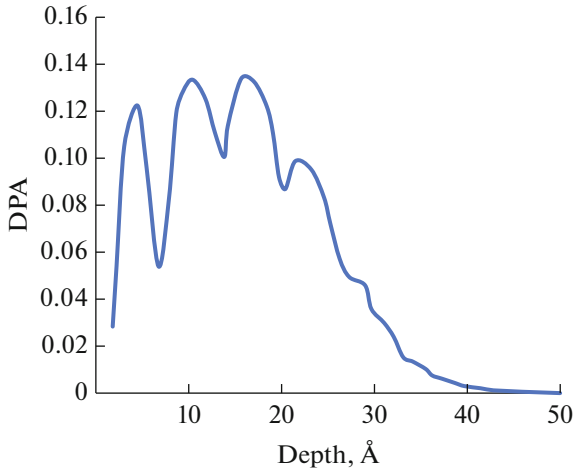

Fig. 7. Profile of destruction of formed defects depending on the depth of the LiF sample under irradiation with Cs ions.

algorithm must be used. Based on Fig. 2, for example, if we need a concentration of cesium impurities of 10^{20} at/cm^3, then the dose of ions Φ will be equal to 1.66×10^{14} cesium/cm^2. If we go from cm^2 to nm^2, we get the value $\Phi = 1.66$ cesium/nm^2. Then, using formula (1), you can obtain DPA—the average number of displaced atoms from a lattice site of a LiF crystal under the influence of bombardment with Cs ions. In Fig. 7 you can see the profile of the destruction of formed defects depending on the depth of the LiF sample when irradiated with Cs ions.

DPA modeling using SRIM was performed in the Kinchin-Pease approximation mode with a threshold displacement energy of 25 eV. Figure 7 shows the damage profile as a function of DPA, where maximum displacement damage peaks are visible at a depth of 16 Å for a Cs ion with an energy of 1 keV, and the range of material damage is within 40 Å. Thus, by determining DPA, we can learn about the damage profile of samples. This means that we can specifically identify which defects are formed and in what depth range of the sample they are located. As seen from Fig. 6, the defect distribution profile does not have a symmetrical shape; at a depth of 40 Å in the sample, the concentration of defects sharply decreases. Such a defect profile shape may be due to lattice deformation and changes in the distance between atoms as a result of ion irradiation. However, it should be noted that the concentration of defects is directly proportional to energy transfer, which initiates damage by displacement. The proportion of displacement damage can be calculated considering the specification of the heavy ion. All data obtained during the experiments are collected in Table 1.

As can be seen from the table, the maximum number of defects when irradiated with Cs ions with an energy of 1 keV is formed at a depth of the LiF sample of 16 Å from the surface and this can be achieved at a dose of $\Phi = 1.66$ ion/nm^2.

Therefore, the displacement cascades formed in the track of the bombarding heavy ion create a significant number of defects. The mass of the bombarding ions directly affects the structural properties of the sample. Consequently, this can be utilized to modify the structural properties of the sample by varying the displacement cross-section.

CONCLUSIONS

The interaction of low-energy 1keV heavy Cs ions with the LiF crystal was analyzed using the SRIM package and demonstrated the possibility of surface modification of the crystal. Here, the average range of cesium ions was 51 Å. Again, the average surface binding energy was obtained as 2.8 eV from the study of changes in sputtering yield depending on recoil energy. The analysis of collision events was also performed in terms of target displacement, vacancies, and substitution collisions, which shows that ion irradiation displaces atoms from their original positions and creates vacancies in the periodic arrangement of the LiF crystal lattice.

The study of the damage profile with displacement through the depth of the sample shows a peak of cre-

Table 1. Irradiation conditions, displacement cross section (σ_{SRIM}), fluence (Φ), and displacement dose (D), electronic energy loss $E(e)$ and nuclear energy loss $E(n)$, cesium ions energy (E)

Target depth, Å	D, dpa	σ_{SRIM}, dpa nm^2	Φ, ion/nm^2	$E(e)$, eV/Å	$E(n)$, eV/Å	E, eV
16	0.13	0.08	1.66	1.7	61.8	1000

ated defects at a depth of 16 Å. Finally, the displacement damage cross-section was obtained based on the displacement of atoms (per 40 Å length) per ion and the atomic density of LiF. Thus, this displacement damage cross-section can be attributed to displacement damage caused by ion irradiation.

Therefore, based on the structural characteristics of the crystal, low-energy heavy ion irradiation can be used to modify the surface of the sample by varying the displacement cross-section. Consequently, LiF crystals can be effectively used as detectors not only in the spectrum of high-energy radiation but also in the spectrum of low-energy ions. Knowledge of the distribution of vacancies, displacement and substitutional defects can serve as an excellent tool for creating *p*–*n*-junctions in semiconductor electronics and radiation technology.

ACKNOWLEDGMENTS

Experiments were partly conducted according to the agreement between St. Petersburg State University and Uzbekistan National Institute for Renewable Energy Sources. Equipment of the Research Park of St. Petersburg State University, "Physical methods of surface investigation" was used within the research presented in the article.

FUNDING

This work was supported by ongoing institutional funding. No additional grants to carry out or direct this particular research were obtained.

CONFLICT OF INTEREST

The authors of this work declare that they have no conflicts of interest.

REFERENCES

1. T. Krasta, I. Manika, A. Kuzmin, J. Maniks, R. Grants, and A. I. Popov, Nucl. Instrum. Methods Phys. Res., Sect. B **545**, 165142 (2023). https://doi.org/10.1016/j.nimb.2023.165142
2. E. Nichelatti, M. Piccinini, P. Nenzi, L. Picardi, C. Ronsivalle, and R. M. Montereali, Nucl. Instrum. Methods Phys. Res., Sect. B **547**, 165207 (2024). https://doi.org/10.1016/j.nimb.2023.165207
3. M. A. Vincenti R M Montereali, F Bonfigli1, et al., J. Phys.: Condens. Matter **36**, 205701 (2024). https://doi.org/10.1088/1361-648X/ad2796
4. R. Vinke, J. Y. Yeom, and C. S. Levin, Phys. Med. Biol. **60** (7), 2785 (2015). https://doi.org/10.1088/0031-9155/60/7/2785
5. A. Cemmi, J. Instrum. **17** (05), T05015 (2022). https://doi.org/10.1088/1748-0221/17/05/T05015
6. U. B. Sharopov, K. Kulwinder, M. K. Qurbanov, et al., Thin Solid Films **735**, 138902 (2021). https://doi.org/10.1016/j.tsf.2021.138902
7. A. Pandey, J. Phys. D. Appl. Phys. **54** (27), 275502 (2021). https://doi.org/10.1088/1361-6463/abf959
8. A. V. Karimov, D. M. Yodgorova, and O. A. Abdulkhaev, J. Eng. Phys. Thermophys. **84** (4), 860 (2011). https://doi.org/10.1007/s10891-011-0543-3
9. Y. Zhou, Electrochem. Solid-State Lett. **9** (3), A147 (2006). https://doi.org/10.1149/1.2162341
10. B. É. Égamberdiev and M. Y. Adylov, Tech. Phys. Lett. **27** (2), 168 (2001). https://doi.org/10.1134/1.1352783
11. B. E. Egamberdiev, Sh. B. Utamurodova, S. A. Tochilin, et al., Appl. Sol. Energy **58** (4), 490 (2022). https://doi.org/10.3103/S0003701X22040065
12. H. Xing, Ping Hu, Shiley Li, et al., J. Mater. Sci. Technol. **62**, 180 (2021). https://doi.org/10.1016/j.jmst.2020.04.063
13. C. Du, Yi. Dai, Hao Hu, et al., Vacuum **222**, 113011 (2024). https://doi.org/10.1016/j.vacuum.2024.113011
14. B. E. Egamberdiyev, S. A. Tachilin, A. R. Toshev, F. M. Isroilov, and M. S. Dehkanov, J. Crit. Rev. **7** (3), 297 (2020). https://doi.org/10.31838/jcr.07.03.60
15. R. R. Bebitov, et al., Low Temp. Phys. **49** (2), 256 (2023). https://doi.org/10.1063/10.0016843
16. B. E. Egamberdiev and A. A. Akbarov, J. Surf. Invest.: X-Ray, Synchrotron Neutron Tech. **15** (3), 611 (2021). https://doi.org/10.1134/S1027451021030241
17. I. Yamada and N. Toyoda, Surf. Coat. Technol. **201** (19), 8579 (2007). https://doi.org/10.1016/j.surfcoat.2006.02.081
18. I. Stabrawa, et al., Vacuum **210**, 111860 (2023). https://doi.org/10.1016/j.vacuum.2023.111860
19. D. G. Liu, S. W. Zhou, J. X. Zou, P. Zhang, Y. Liang, and C. F. Hong, Vacuum **217**, 112538 (2023). https://doi.org/10.1016/j.vacuum.2023.112538
20. U. B. Sharopov, K. Kaur, M. K. Kurbanov, D. S. Saidov, E. T. Juraev, and M. M. Sharipov, Silicon **14** (9), 4661 (2022). https://doi.org/10.1007/s12633-021-01268-0
21. M. Rubel, J. P. Coad, and D. Hole, Vacuum **78** (2–4), 255 (2005). https://doi.org/10.1016/j.vacuum.2005.01.109
22. D. Nath and R. Das, Vacuum **190**, 110293 (2021). https://doi.org/10.1016/j.vacuum.2021.110293
23. S. Kalia, R. Kumar, R. Dhiman, and R. K. Singh, J. Energy Storage **83**, 110650 (2024). https://doi.org/10.1016/j.est.2024.110650
24. B. E. Egamberdiev, N. T. Rustamov, A. S. Mallaev, and A. M. Norov, J. Surf. Invest.: X-Ray, Synchrotron Neutron Tech. **9** (3), 612 (2015). https://doi.org/10.1134/S1027451015030222
25. U. B. Sharopov, B. G. Atabaev, R. Djabberganov, and M. K. Kurbanov, J. Surf. Invest.: X-Ray, Synchrotron Neutron Tech. **7** (1), 195 (2013). https://doi.org/10.1134/S1027451012120117

26. A. B. Rech, A. Kinoshita, P. M. Donate, and O. Baffa, Appl. Radiat. Isot. **181**, 110105 (2022). https://doi.org/10.1016/j.apradiso.2022.110105
27. J. E. Ngaile and W. E. Muhogora, J. Radiol. Prot. **24** (2), 155 (2004). https://doi.org/10.1088/0952-4746/24/2/005
28. N. Kawaguchi, G. Okada, and T. Yanagida, ECS Meet. Abstr. **MA2016-02** (42), 3162 (2016). https://doi.org/10.1149/MA2016-02/42/3162
29. R. M. Montereali, E. Nichelatti, M. Piccinini, V. Nigro, and M. A. Vincenti, J. Solid State Sci. Technol. **10** (11), 116001 (2021). https://doi.org/10.1149/2162-8777/ac31cc
30. D. Nath, F. Singh, and R. Das, Mater. Sci. Semicond. Process. **114**, 105079 (2020). https://doi.org/10.1016/j.mssp.2020.105079
31. B. A. Abdurakhmanov, K. M. Iliev, S. A. Tachilin, A. R. Toshev, and B. E. Egamberdiev, Surf. Eng. Appl. Electrochem. **46** (5), 505 (2010). https://doi.org/10.3103/S1068375510050170
32. U. Sharopov, et al., Radiat. Eff. Defects Solids **178** (5–6), 539 (2023). https://doi.org/10.1080/10420150.2022.2133716
33. U. B. Sharopov, B. G. Atabaev, R. Djabbarganov, M. K. Kurbanov, and M. M. Sharipov, J. Surf. Invest.: X-Ray, Synchrotron Neutron Tech. **10** (1), 24 (2016). https://doi.org/10.1134/S1027451016010328
34. Y. Kudriavtsev and R. Asomoza, Vacuum **194**,110592 (2021). https://doi.org/10.1016/j.vacuum.2021.110592
35. M. K. Karimov, F. O. Kuryozov, S. R. Sadullaev, M. U. Otabaev, and S. B. Bobojonova, Mater. Sci. Forum **1049**, 192 (2022). https://doi.org/10.4028/www.scientific.net/MSF.1049.192
36. M. K. Karimov, U. O. Kutliev, S. B. Bobojonova, and K. U. Otabaeva, Phys. Chem. Solid State **22** (4), 742 (2021). https://doi.org/10.15330/pcss.22.4.742-745
37. J. Leveneur, Y. Zhang, H. Fiedler, S. Prabakar, E. C. Le Ru, and J. Kennedy, Surf. Coat. Technol. **468**, 129768 (2023). https://doi.org/10.1016/j.surfcoat.2023.129768
38. J. Jussila, F. Granberg, and K. Nordlund, Nucl. Mater. Energy **17**, 113 (2018). https://doi.org/10.1016/j.nme.2018.08.002
39. U. Sharopov, et al., Vacuum **213**, 112133 (2023). https://doi.org/10.1016/j.vacuum.2023.112133
40. J. F. Ziegler, M. D. Ziegler, and J. P. Biersack, Nucl. Instrum. Methods Phys. Res., Sect. B **268** (11–12), 1818 (2010). https://doi.org/10.1016/j.nimb.2010.02.091
41. G. H. Kinchin and R. S. Pease, Reports Prog. Phys. **18** (1), 301 (1955). https://doi.org/10.1088/0034-4885/18/1/301
42. J. F. Ziegler, Nucl. Instrum. Methods Phys. Res., Sect. B **219–220**, 1027 (2004). https://doi.org/10.1016/j.nimb.2004.01.208
43. P. Sigmund, Thin Solid Films **520** (19), 6031 (2012). https://doi.org/10.1016/j.tsf.2012.06.003
44. J. Guo, Argonne, IL, Jun. (1993). https://doi.org/10.2172/46692